© 2019. Published by The Company of Biologists Ltd | Journal of Experimental Biology (2019) 222, jeb204305. doi:10.1242/jeb.204305

RESEARCH ARTICLE

Ground reaction forces intersect above the center of mass even when walking down visible and camouflaged curbs

Johanna Vielemeyer[1,2,*], Eric Grießbach[2] and Roy Müller[1,2]

ABSTRACT

A main objective in bipedal walking is controlling the whole body to stay upright. One strategy that promotes this objective is to direct the ground reaction forces (GRFs) to a point above the center of mass (COM). In humans, such force patterns can be observed for unperturbed walking, but it is not known whether the same strategy is used for a walkway that changes in height. In this study, 11 volunteers stepped down off a visible (0, 10 and 20 cm) and a camouflaged (0 or 10 cm) curb while walking at two different speeds (1.2±0.1 and 1.7±0.1 m s^{-1}). The results showed that in all conditions the GRFs pointed predominantly above the COM. Vectors directed from the center of pressure (COP) to the intersection point (IP) closely fitted the measured GRF direction not only in visible conditions (R^2>97.5%) but also in camouflaged curb negotiation (R^2>89.8%). Additional analysis of variables included in the calculation of the IP location showed considerable differences for the camouflaged curb negotiation: compared with level walking, the COP shifted posterior relative to the COM and the vertical GRFs were higher in the beginning and lower in later parts of the stance phase of the perturbed contact. The results suggest that IP behavior can be observed for both visible and camouflaged curb negotiation. For further regulation of the whole-body angle, the asymmetrical vertical GRFs could counteract the effect of a posterior shifted step.

KEY WORDS: Angular momentum, Bipedal gait, Perturbation, Stability, Uneven ground, Virtual pivot point

INTRODUCTION

Walking is widely present in human everyday life, but it is nonetheless a complex task for the neural and mechanical systems (Capaday, 2002; Gruben and Boehm, 2012a; Nielsen, 2003; Winter, 1995, 2009). Maintaining an upright position and thus controlling the whole-body angle is challenging. Hence, the angular momentum of the whole body seems to be highly controlled when walking (Herr and Popovic, 2008). If the regulation of the upright position is perturbed, e.g. by stumbling over obstacles (Pijnappels et al., 2004) or stepping down unexpected (van Dieën et al., 2007) or camouflaged (Müller et al., 2014) changes in ground level, it may lead to falls or fall-related injuries, particularly in the elderly (e.g. Berg et al., 1997; Menz et al., 2003; Pijnappels et al., 2005). Therefore, the use of a model or the analysis of specific target variables to describe walking characteristics can be important tools to understand the mechanism of stability (e.g. Alexander, 1995; Roos and Dingwell, 2013).

[1]Klinikum Bayreuth GmbH, 95445 Bayreuth, Germany. [2]Friedrich-Schiller-University Jena, 07737 Jena, Germany.

*Author for correspondence (johanna.vielemeyer@uni-jena.de)

J.V., 0000-0003-1282-3576; R.M., 0000-0002-4688-1515

Received 4 April 2019; Accepted 24 June 2019

A mechanical strategy to stabilize the body while walking is to direct the forces to a point above the center of mass of the whole body (COM). Based on this, in the virtual pivot concept the body is conceived like a pendulum with a single rigid mass representing the trunk along with massless legs (Maus et al., 2010). In this model, a trunk-fixed virtual pivot point (VPP) is the target variable controlling the direction of the ground reaction forces (GRFs). However, the fluctuations of the model's trunk pitch angle were 180 deg out of phase with the upper body angle of humans (Gruben and Boehm, 2012a; Müller et al., 2017). A physical model with the appropriate phase relationship between GRF behavior and whole-body motion is a rocking rigid block. However, that model would predict an intersection point (IP) with a fixed height (Gruben and Boehm, 2012a). The general idea for the stabilizing effect is that across time the GRFs can provide a torque around the lateral axis in the upright direction (Lee et al., 2017).

In human walking, a stabilizing strategy based on neural control seems to generate such an IP of GRFs. This point has been examined in various studies, at least in the sagittal plane, but named differently [e.g. VPP in Maus et al. (2010) or divergent point (DP) in Gruben and Boehm (2012a)]. The studies showed that such a point seems to be important for controlling upright walking, because different environmental situations and perturbations during walking can be compensated for to some degree (Gruben and Boehm, 2012a; Maus et al., 2008, 2010). However, the vertical position of the IP seems to show a high variance between and within the studies, possibly related to the different walking speeds used (Müller et al., 2017).

In addition to speed, other factors may affect the position of the IP. In this context, Müller et al. (2017) studied walking with altered trunk orientations (see also Aminiaghdam et al., 2017). For this internal (body-related), geometrical perturbation, the data still suggest that the GRFs intersect near a point above the COM, although with greater spread of the force vectors around this point than in upright walking. In addition to internal perturbations, external (environment-related) perturbations such as ground level changes (e.g. gaps in the ground, curbs or stairs) may also cause alterations in the gait pattern. These alterations have been biomechanically well studied (e.g. van Dieën et al., 2008; Müller et al., 2014; Peng et al., 2016; Reeves et al., 2008; Silverman et al., 2014), but not with a focus on an IP. That consideration is worthwhile, notably because the simulation of the VPP showed a stabilizing effect only for a small perturbation such as a 5 mm curb (Maus et al., 2010).

Furthermore, unexpected level changes while walking, e.g. when a curb is not noticed, often lead to falls (Berg et al., 1997). Possibly as a result of a lack of anticipative adaptations, such perturbation may place high demands on the regulation of linear momentum and angular momentum in order to avoid falling (Buckley et al., 2008). For example, van Dieën et al. (2007) observed that the sum over time of the angular momenta of the whole body during a stride while stepping down off a camouflaged curb is smaller than for level

Journal of Experimental Biology (2019) 222, jeb204305. doi:10.1242/jeb.204305

List of symbols and abbreviations

bw	body weight
C10	camouflaged curb of 10 cm
COM	center of mass of the whole body
COM_z	vertical COP-centered COM position
COP	center of pressure
$COP_{10,x}$	horizontal COM-centered COP position at 10% of the stance phase
$COP_{90,x}$	horizontal COM-centered COP position at 90% of the stance phase
DP	divergent point
g	standard gravity
GRFs	ground reaction forces
IP	intersection point
IP_x	horizontal IP position
IP_z	vertical IP position
l	distance between lateral malleolus and trochanter major of the leading leg
L_{wb}	angular momentum of the whole body
$N_{\%}$	number of gait percentage times analyzed
N_{trial}	number of trials
$\vec{p}_{brake,x}$	horizontal braking impulse
$\vec{p}_{brake,z}$	vertical braking impulse
$\vec{p}_{normalized}$	normalized impulse
$\vec{p}_{prop,x}$	horizontal propulsion impulse
$\vec{p}_{prop,z}$	vertical propulsion impulse
R^2	coefficient of determination
TD	touchdown
t_{double}	double stance time
TO	take-off
V0	visible curb of 0 cm
V10	visible curb of 10 cm
V20	visible curb of 20 cm
VPP	virtual pivot point
γ_{wb}	whole-body angle
$\gamma_{wb,10}$	whole-body angle at 10% of the stance phase
$\gamma_{wb,90}$	whole-body angle at 90% of the stance phase
θ	angle between the model forces and the GRFs
θ_{Exp}	angle of the experimentally measured GRFs in the sagittal plane
$\overline{\theta}_{Exp}$	mean experimental angle of GRFs
θ_{Mod}	angle of the model forces

walking, thus resulting in a more clockwise rotation of the body. Not falling means that there is a strategy to keep the balance and that kinetic and kinematic adjustments are made (Müller et al., 2014). Nevertheless, stepping down off a curb has not been investigated in the context of whole-body angle or IP regulation. The IP control is a supportive strategy, but neither necessary nor sufficient to stay upright; hence, there could be other strategies (Gruben and Boehm, 2012a).

Based on these considerations, it is possible that during camouflaged curb negotiation the stabilizing IP control is lost and the GRFs do not intersect near a point anymore or the IP is not found above the COM. However, we hypothesize that both for visible and camouflaged curb negotiation, the GRFs intersect above the COM. Additionally, we assume that the deviation of the measured GRF lines of action from the calculated IP is larger in the camouflaged than in the visible walking conditions.

MATERIALS AND METHODS

Subjects

Eleven volunteers (3 female, 8 male; mean±s.d., age: 25.8±4.8 years, mass: 68.3±8.1 kg, height: 178.9±9.4 cm) took part in this experiment. Because of missing data regarding the COM, which is necessary for the IP calculation, only 10 of the 11 subjects were considered in the evaluation. All of them were physically active and had no known restrictions which could have affected their performance or behavior in the study. Prior to participation, an informed consent form was signed by each subject. The experiment was approved by the local ethics committee (University of Jena, 3532-08/12) and conducted in accordance with the Declaration of Helsinki.

Measurements

The subjects were asked to walk along an 8 m walkway with two consecutive force plates in its center (Fig. 1). They were instructed to reach the first force plate with the left foot (trailing leg) and the second force plate with the right foot (leading leg) while walking with two different constant speeds: slow (1.2±0.1 m s^{-1}) and fast (1.7±0.1 m s^{-1}), as controlled by an examiner. To comply with the requirements, several practice trials took place before beginning the experiment. The force plate of the first contact (9281B, Kistler, Winterthur, Switzerland) was fixed at ground level for the first part of the walkway. The force plate of the second contact (9287BA, Kistler) was adjustable in height, as was the subsequent part of the walkway. The GRFs of both force plates were sampled at 960 Hz.

First, the subjects had to walk over three visible settings: for one, the track was even (V0, visible level); for the other two, the force plate on the second contact and the subsequent walkway were both lowered by either 10 cm (V10, visible curb of 10 cm) or 20 cm (V20, visible curb of 20 cm). The order of the settings was block randomized as well as the order of the walking speed for each

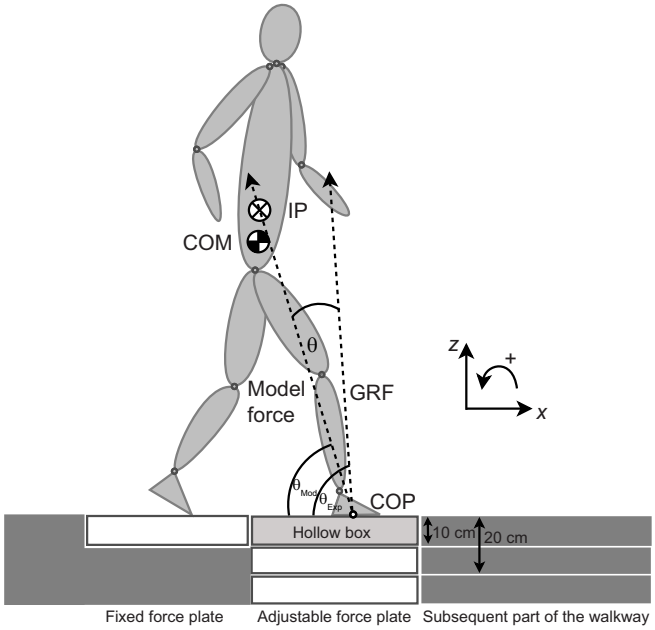

Fig. 1. Side view of the walkway. In the visible conditions, the second force plate (adjustable) and the subsequent walkway were set at elevations of 0 cm (V0, visible level), −10 cm (V10, visible curb of 10 cm) and −20 cm (V20, visible curb of 20 cm) relative to the first force plate (fixed). For the camouflaged curb negotiation, a 10 cm high block was randomly either present or absent on the adjustable force plate (10 cm below the fixed force plate). The block was camouflaged with a hollow box covered with an opaque sheet of paper (light gray rectangle). Here, the subsequent walkway was always set at an elevation of −10 cm. The model force goes through the center of pressure (COP) and the calculated intersection point (IP). The angle θ is between the model force vector and the measured ground reaction force (GRF) vector for each time frame ($\theta=\theta_{Exp}-\theta_{Mod}$). COM is the center of mass of the whole body.

setting. In each visible condition, the subjects had to accomplish eight trials. Thereafter, for the camouflaged setting, the basic setup was the same as for the V10 condition but a wooden block with a height of 10 cm was randomly either present or absent on the force plate of the second contact; the top surface was camouflaged with an opaque sheet of paper, so that the subjects did not know whether they were stepping down 10 cm (C10, camouflaged curb of 10 cm) or walking one more step on the same level before stepping down. In the camouflaged setting, the participants had to accomplish 10 trials at each velocity, while the order of the four block-absent and six block-present trials was randomized. A trial (visible or camouflaged) was only analyzed when the subject hit the corresponding force plates with the correct foot without losing any reflective joint markers. The spherical markers (19 mm diameter) were placed on the tip of the fifth toe, lateral malleolus, epicondylus lateralis femoris, trochanter major, anterior superior iliac spine, acromion, epicondylus lateralis humeri and ulnar styloid processus on both sides of the body as well as on L5 and C7 process spinosus.

All trials were recorded with eight cameras (240 Hz) by a 3D infrared system (MCU 1000, Qualisys, Gothenburg, Sweden) and synchronized using the trigger of the Kistler software and hardware (for more details regarding the experimental setup, see AminiAghdam et al., 2019).

Data processing

All data were analyzed with custom-written Matlab codes (The Mathworks, Inc., Natick, MA, USA). The raw kinetic data were filtered at a 50 Hz cut-off frequency and kinematic data were filtered at 12 Hz with a bidirectional fourth-order low-pass Butterworth filter. Kinetic data were normalized by individual body weight (bw). The moments of touchdown (TD) and take-off (TO) were calculated as the instants when the GRFs exceeded or fell below the threshold of 0.02 bw, respectively, for first and second contacts. The COM was determined with a body segment parameters method according to Plagenhoef et al. (1983).

To compute the IP, we used the GRF vectors starting in the center of pressure (COP) for every instant of measurement in a COM-centered coordinate frame, where the vertical axis is parallel to gravity, as delineated by Müller et al. (2017). The chosen reference frame was evaluated by Gruben and Boehm (2012a) because of the mechanical significance of the COM and the omnipresence of the gravity force field. Although other examined reference frames provided significantly better predictions of the DP model, the quality was nevertheless high in all reference frames (Gruben and Boehm, 2012a). Therefore, in this study the COM-centered coordinate system was chosen because of its simple linking to the angular momentum of the whole body. The position of the IP with respect to the COM is the point where the sum of the squared perpendicular distances to the GRFs from 10% to 90% of stance is minimal. This time frame of 80% of the stance phase was chosen based on the literature (Andrada et al., 2014; Müller et al., 2017) to make the different conditions more comparable, because the double stance time (t_{double}) varied (see below). As the data were normalized to 250 samples per stance phase per trial, 200 samples of measured GRF lines of action were included in the calculation. The IP was computed only for the second (perturbed) contact, separately for each trial. Because the COP could not be determined exactly in the block-present condition, the IP was not calculated here.

The calculated model forces go through the COP and the computed IP (Fig. 1). To estimate the amount of agreement between model forces and experimentally measured GRFs, we considered the angle of the GRF θ_{Exp} and of the model forces θ_{Mod} for each trial (N_{trial}=8 for visible conditions and N_{trial}=4 for camouflaged conditions, respectively) and measurement time ($N_{\%}$=100). The mean experimental angle $\bar{\theta}_{Exp}$ is the mean over all trials and measurement times. Based on this, we calculated the coefficient of determination R^2, as suggested by Herr and Popovic (2008):

$$R^2 = \left(1 - \frac{\sum_{i=1}^{N_{trial}} \sum_{j=1}^{N_{\%}} \left(\theta_{Exp}^{ij} - \theta_{Mod}^{ij}\right)^2}{\sum_{i=1}^{N_{trial}} \sum_{j=1}^{N_{\%}} \left(\theta_{Exp}^{ij} - \bar{\theta}_{Exp}\right)^2}\right) \times 100\%. \quad (1)$$

Note that R^2=100% would mean that the angle of the GRFs and the angle of the model forces match for each trial and each measurement time. An R^2 value of 0% or smaller would mean that the estimation of the model is equal to or even worse than the use of $\bar{\theta}_{Exp}$ as an estimate (Herr and Popovic, 2008). We also calculated the angle θ between the model forces and the GRFs (Fig. 1) for each measurement time to quantify the force difference over time.

To determine changes in variables needed for IP calculations (IP-related variables), we also computed horizontal and vertical impulses $\vec{p}$ for two time intervals (braking and propulsion) as the integrals of the GRFs. The braking interval went from TD to zero-crossing of the horizontal GRFs and the propulsion interval from the zero-crossing of the horizontal GRFs to TO, respectively. For better comparability, impulses were normalized to each subject's body weight bw, leg length l (distance between lateral malleolus and trochanter major of the leading leg) and standard gravity $\boldsymbol{g}$ as denoted in Eqn 2 (Hof, 1996):

$$\vec{p}_{normalized} = \frac{\vec{p}}{bw \cdot \sqrt{l/\boldsymbol{g}}}. \quad (2)$$

As an additional variable, the angular momentum of the whole body $\mathbf{L}_{wb}$ was calculated as the sum of individual segment angular momenta about the COM (Herr and Popovic, 2008) and was normalized to each subject's body weight and the mean vertical COM position of the fast visible level walking to reduce data variance between the subjects (Herr and Popovic, 2008). The whole-body angle γ_{wb} was determined as the integral of the non-normalized angular momentum. The integration constant was chosen so that γ_{wb} was zero at mid-stance of the trailing leg in the step before perturbation. Mid-stance was defined as the frame when the COM was above the lateral malleolus.

To compare IP variables, IP-related variables and additional variables, we used repeated measures ANOVA (P<0.05; SPSS®, Chicago, IL, USA) with *post hoc* analysis (Šidák correction) regarding the factors 'speed' (slow and fast) and 'ground condition' (V0, V10, V20, C10). To analyze whether the IP was above the COM, we performed a one-sample *t*-test compared with zero (separately for each condition with Šidák correction).

RESULTS

The results and statistical values of 10 subjects are listed in Table 1 and illustrated in Figs 2–6. Figs 2–4 show IP variables, Fig. 5 shows IP-related variables and Fig. 6 shows additional variables. For clarity, only data for the fast conditions are shown in Figs 4–6. Figures for the slow conditions differ only slightly from those of the fast conditions (see Figs S1 and S2). Additionally, significant mean differences will be highlighted in the following sections of the Results.

Journal of Experimental Biology (2019) 222, jeb204305. doi:10.1242/jeb.204305

Table 1. Statistical analysis of investigated IP parameters

		Ground condition				*P*-value *F*-value/η^2		
	Speed	V0	V10	V20	C10	Ground	Speed	Interaction
IP variables								
IP_x (cm)	Slow	0.3±1.1	−0.2±1.8	0.7±1.2 [a]	−2.7±1.8 [a,b]	**0.000**	**0.001**	0.269
	Fast	−1.4±2.1	−1.2±2.1	−0.3±1.4 [a]	−3.5±2.0 [a,b]	73.62/0.89	22.10/0.71	1.42/0.14
IP_z (cm)	Slow	18.5±5.7	13.2±6.3 [a]	9.9±6.2 [a]	19.7±11.4	**0.026**	0.563	0.436
	Fast	15.0±4.8	11.8±5.3 [a]	11.9±7.6 [a]	19.5±16.7	6.12/0.41	0.36/0.04	0.74/0.08
R^2 (%)	Slow	97.7±0.9	97.9±0.9	98.1±0.8	94.6±2.9[a]	0.000	0.013	**0.013**
	Fast	97.5±1.0	97.9±1.0	97.6±0.9	89.8±5.3[a,b]	24.66/0.73	9.67/0.52	9.19/0.51
IP-related variables								
$COP_{10,x}$ (m)	Slow	0.31±0.02	0.27±0.02	0.27±0.03 [a]	0.20±0.04 [a,b]	**0.000**	**0.034**	0.077
	Fast	0.33±0.02	0.30±0.03	0.28±0.04 [a]	0.19±0.02 [a,b]	60.62/0.87	6.21/0.41	3.47/0.28
$COP_{90,x}$ (m)	Slow	−0.28±0.02	−0.30±0.03 [a]	−0.32±0.02 [a]	−0.36±0.03 [a,b]	**0.000**	**0.000**	0.383
	Fast	−0.32±0.02	−0.35±0.03 [a]	−0.37±0.03 [a]	−0.40±0.06 [a,b]	28.48/0.76	32.40/0.78	0.95/0.10
$\vec{p}_{brake,x}$	Slow	−0.14±0.02	−0.16±0.02[a]	−0.15±0.02	−0.11±0.02[a,b]	0.000	0.458	**0.000**
	Fast	−0.15±0.01	−0.18±0.02[a]	−0.15±0.03	−0.09±0.02[a,b]	38.15/0.81	0.60/0.06	14.13/0.61
$\vec{p}_{prop,x}$	Slow	0.13±0.02	0.13±0.02	0.15±0.03	0.10±0.03[a,b]	0.000	0.003	**0.014**
	Fast	0.12±0.02	0.13±0.01	0.13±0.03	0.08±0.03[a,b]	34.81/0.78	16.34/0.65	4.25/0.32
$\vec{p}_{brake,z}$	Slow	1.15±0.08	1.24±0.08[a]	1.21±0.07	1.12±0.07	0.000	0.000	**0.017**
	Fast	1.00±0.05	1.10±0.04[a]	1.13±0.06[a]	0.94±0.10[b]	11.90/0.57	47.80/0.84	4.03/0.31
$\vec{p}_{prop,z}$	Slow	0.99±0.09	0.85±0.05[a]	0.91±0.08	0.71±0.10[a,b]	0.000	0.000	**0.007**
	Fast	0.76±0.06	0.70±0.05[a]	0.67±0.06[a]	0.55±0.10[a,b]	31.12/0.78	465.27/0.98	5.03/0.36
Additional variables								
$\gamma_{wb,10}$ (deg)	Slow	−0.30±0.11	−0.59±0.14[a]	−0.73±0.20[a]	−0.99±0.14[a,b]	0.000	0.000	**0.002**
	Fast	−0.31±0.06	−0.65±0.13[a]	0.96±0.14[a,b]	−1.09±0.15[a,b]	64.30/0.88	29.40/0.77	6.67/0.43
$\gamma_{wb,90}$ (deg)	Slow	−0.48±0.14	−0.68±0.07 [a]	−0.90±0.10 [a,b]	−1.34±0.22 [a,b]	**0.000**	0.491	0.539
	Fast	−0.46±0.11	−0.66±0.11 [a]	−0.98±0.19 [a,b]	−1.37±0.39 [a,b]	73.31/0.89	0.52/0.05	0.53/0.06

V0, visible level walking; V10,20, visible curb of 10 or 20 cm; C10, camouflaged curb of 10 cm; IP, horizontal (*x*) and vertical (*z*) positions of the intersection point relative to the center of mass (COM); R^2, coefficient of determination of the angles between measured ground reaction forces (GRFs) and model forces [through center of pressure (COP) and IP]; $COP_{10,x}$,$COP_{90,x}$, horizontal COM-centered COP position at 10% or 90% of stance phase; $\vec{p}_{brake}$, braking impulse in the *x*- and *z*-direction; $\vec{p}_{prop}$, propulsion impulse in the *x*- and *z*-direction; γ_{wb}, whole-body angle at 10% and 90% of stance phase.
Data are means±s.d. across all included subjects (N=10). *Post hoc* analysis with Šidák correction revealed significant differences between ground conditions: differences from V0 and V10 are indicated with 'a' and 'b', respectively (P<0.05). The same denotation is used for the interaction, here across each speed. Underlined values indicate a significant difference from the slow walking speed condition. Bold indicates P<0.05.

IP variables

In the visible conditions, the IP height decreased with a larger curb drop. However, the IP was always above the COM. The R^2 was high in all conditions, but significantly lower in the camouflaged compared with the visible conditions.

The horizontal IP position (IP_x) showed a significant main effect for ground condition and speed (Table 1). In V20, the IP_x was 0.8 cm more posterior than in V0 (P=0.027). In the camouflaged condition (C10), it was 2.6 and 2.4 cm more posterior compared with V0 and V10 (P<0.001). In fast walking, the IP_x was 1.1 cm more posterior. The vertical IP position (IP_z; Fig. 3A) showed a significant main effect for ground condition. It was 4.3 cm lower in V10 (P=0.001) and 5.9 cm lower in V20 (P=0.002) compared with V0. There were no significant differences between C10 and the visible conditions nor speed effects in any conditions. The IP_z was in all conditions significantly above the COM (P≤0.039). In Fig. 2, exemplary illustrations of the IP for single trials of different subjects are shown.

In R^2 (Fig. 3B), there was an interaction between ground condition and speed (Table 1). The mean value in C10 was 3.1 and 7.7 percentage points lower than in V0 (slow: P=0.033; fast: P=0.025). Additionally, in fast walking, the R^2 in C10 was 8.1 percentage points lower than in V10 (P=0.025). However, at fast C10, the variance between subjects was high, with 76.1% being the lowest and 95.3% being the highest value (Fig. 3B). In V20, R^2 was 0.5 percentage points lower in fast walking (P=0.017). The generally high R^2 mean values (89.8–98.1%) indicate good agreement between model forces and measured forces and therefore a small angle θ between them.

The absolute value of the angle θ between model forces and GRFs was in some cases more than 3 times higher in the first and the

Table 2. Walking velocity and double stance time (t_{double})

		Ground condition				*P*-value *F*-value/η^2		
	Speed	V0	V10	V20	C10	Ground	Speed	Interaction
Velocity (m s^{-1})	Slow	1.17±0.07	1.21±0.07	1.20±0.08	1.28±0.08 [a]	**0.002**	**0.000**	0.780
	Fast	1.66±0.09	1.68±0.13	1.70±0.08	1.77±0.15 [a]	6.39/0.42	385.56/0.98	0.36/0.04
t_{double} (s)	Slow	0.14±0.01	0.12±0.01 [a]	0.10±0.01 [a,b]	0.04±0.02 [a,b]	**0.000**	**0.000**	0.060
	Fast	0.10±0.01	0.09±0.01 [a]	0.07±0.01 [a,b]	0.02±0.09 [a,b]	167.47/0.95	231.54/0.96	4.24/0.32

Data are means±s.d. across all included subjects (N=10). *Post hoc* analysis with Šidák correction revealed significant differences between ground conditions: differences from V0 and V10 are indicated with 'a' and 'b', respectively (P<0.05). The same denotation is used for the interaction, here across each speed. Underlined values indicate a significant difference from the slow walking speed condition. Bold indicates P<0.05.

Journal of Experimental Biology (2019) 222, jeb204305. doi:10.1242/jeb.204305

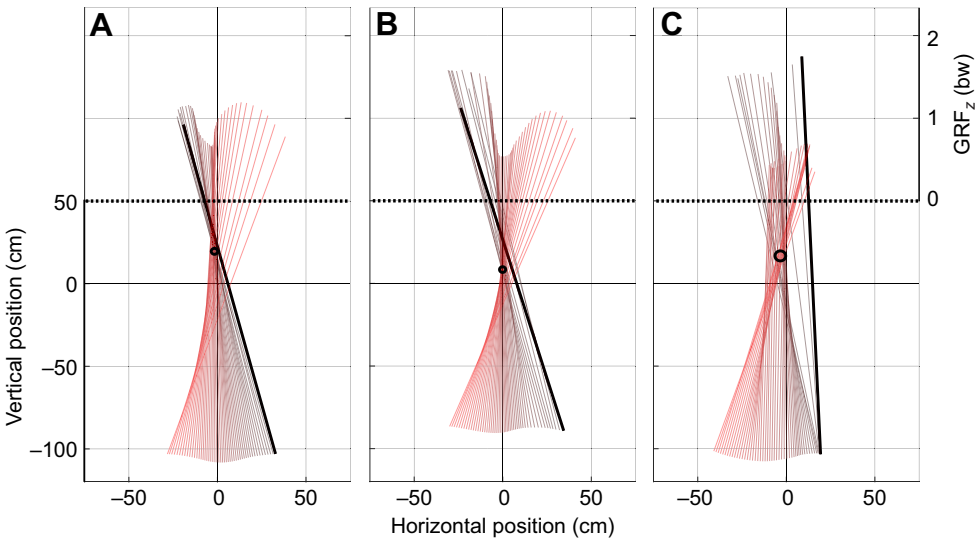

Fig. 2. Examples of the IP in a COM-centered coordinate system for different subjects and conditions. Lines show the GRFs at different measurement times (10–90% of the single support phase; black to red, thicker line indicates the first vector), originating at the COP. The midpoints of the circles indicate the calculated IP; the radii represent the mean spread of the GRFs relative to the IP. (A) Fast visible level walking (V0). (B) Fast walking with a visible curb of 10 cm (V10). (C) Fast walking with a camouflaged curb of 10 cm (C10). For each condition, the trial with the spread around the IP nearest to the 50th percentile of all subjects was chosen. Above 50 cm, the vertical length of the vector represents the vertical GRF. Animated versions of these graphs can be found in the supplementary information (Movies 1–3).

last 10% of the stance phase than in the remaining 80% (Fig. 4). There, θ did not exceed 6 deg in any condition; the highest values were reached at the beginning and at the end of the single stance phase. The angle of C10 was almost always larger than that of the other conditions.

IP-related variables

The horizontal COP shifted in the posterior direction with a larger curb drop and from visible to camouflaged conditions. From visible level to 10 cm curb walking, the braking impulses increased and the vertical propulsion impulses decreased. In the camouflaged condition, the impulses became smaller compared with those for visible level walking.

The horizontal position of the COM-referenced COP showed significant main effects for ground condition and speed for both 10% and 90% of the stance phase (Table 1). The COP was, relative to the COM, significantly more posterior in all curb conditions compared with V0, for both 10% (except V10; V20: −4.5 cm, P=0.020; C10: −12.5 cm, P<0.001) and 90% (V10: −2.5 cm, P=0.004; V20: −4.5 cm, P=0.001; C10: −8.0 cm, P=0.025). Additionally, the COP was more posterior for C10 compared with V10 (10%: −9.0 cm, P<0.001; 90%: −5.5 cm, P=0.035). Fig. 5A shows that the horizontal COP was more posterior for larger curb heights and for camouflaged compared with visible conditions for the whole stance phase. In fast walking, $COP_{10,x}$ was 2.0 cm more anterior in the visible conditions and 1.0 cm more posterior in C10 compared with that in slow walking. $COP_{90,x}$ was 4.5 cm more posterior in fast walking. The COM_z position with respect to the floor showed only minor differences between the conditions (Fig. 5B).

For the horizontal and vertical impulse $\vec{p}_{brake}$ and $\vec{p}_{prop}$, there was an interaction between ground condition and speed (Table 1). The horizontal braking impulse was significantly larger in V10 than in V0 (slow: P=0.004; fast: P=0.033). It was lower in C10 than in V0 (slow: P=0.010; fast: P<0.001) and in V10 (P<0.001). In V0 and V10, it was larger (P≤0.040), and in C10 it was lower (P=0.016) for fast walking. The horizontal propulsion impulse was significantly lower in C10 than in V0 (P≤0.021) and V10 (P≤0.035). The horizontal forces for each condition for fast walking are shown in Fig. 5C. In V20 and C10, GRF_x was smaller for fast walking. The vertical impulse during the braking phase $\vec{p}_{brake,z}$ was larger in V10 than in V0 (P≤0.024). In fast walking, it was larger in V20 than in V0 (P=0.011) and lower in C10 than in V10 (P=0.019). The vertical impulse during the propulsion phase $\vec{p}_{prop,z}$ was lower in all curb conditions than in V0 (P≤0.031), except for the slow V20. In C10, it was lower than in V10 (P≤0.007). In all conditions, $\vec{p}_{brake,z}$ and $\vec{p}_{prop,z}$ were lower in fast walking (P≤0.001). Fig. 5D suggests that $\vec{p}_{prop,z}$ increased and $\vec{p}_{brake,z}$ decreased with the lower visible curb condition and even more so in C10 compared with the visible conditions. Therefore, GRF_z became more asymmetrical.

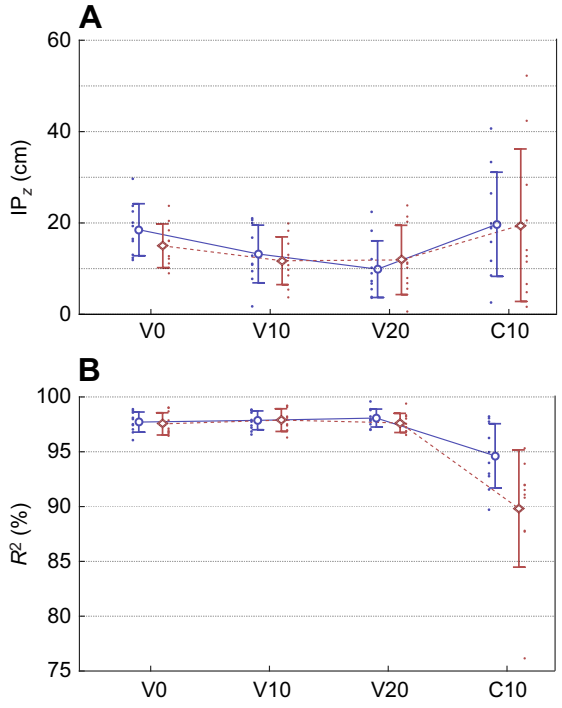

Fig. 3. Mean±s.d. IP variables between subjects for each walking condition (V0, V10, V20 and C10). Blue circles indicate slow walking and red diamonds indicate fast walking. (A) Vertical position of the intersection point (IP_z) relative to the COM. Each dot is the median over all trials of one condition for one subject. (B) R^2 represents the ratio of the angle between measured and model forces and their variance. Each dot represents one subject. Notice that the R^2 value of one subject is strikingly lower in fast C10.

Journal of Experimental Biology (2019) 222, jeb204305. doi:10.1242/jeb.204305

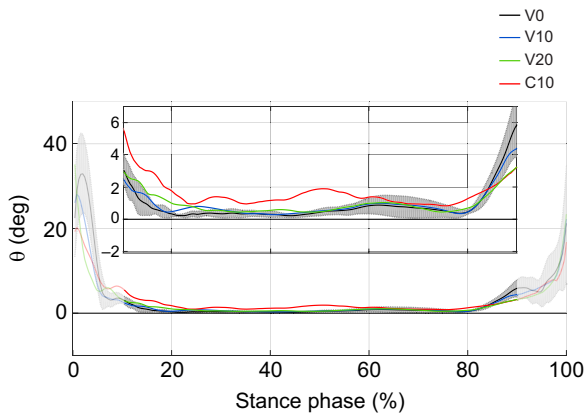

Fig. 4. Absolute angle θ between model forces and GRFs. Mean (±s.d. for visible level walking, V0) data across the subjects (*N*=10) for fast conditions (V0, V10, V20 and C10). The darker curve representing 10–90% of stance phase of the leading leg is shown on an enlarged scale in the inset.

Additional variables

The angular momentum in the camouflaged condition differed from that in the other conditions. Additionally, the subjects rotated more anterior with a larger curb drop and from visible to camouflaged conditions. However, the differences were smaller than 2 deg.

The angular momentum in the sagittal plane $\mathbf{L}_{wb}$ differed between the conditions before the stance phase of the leading leg (Fig. 6A). In the visible conditions, $\mathbf{L}_{wb}$ increased with the larger curb height around the TD of the leading leg. However, shortly after, the TO of the trailing leg $\mathbf{L}_{wb}$ was similar for all conditions. Only in C10 was there a larger $\mathbf{L}_{wb}$ after the TO in the posterior direction and thereafter a larger $\mathbf{L}_{wb}$ in the anterior direction compared with the visible conditions, like an overshoot. In all conditions, a deficit in $\mathbf{L}_{wb}$ over the whole stride and the subsequent double stance phase (extended stride) could be observed.

The range of the whole-body angle γ_{wb} did not exceed 2 deg. For $\gamma_{wb,10}$ in the sagittal plane, there was an interaction between ground condition and speed (Table 1). $\gamma_{wb,10}$ in all curb conditions was significantly larger than in V0 (mean difference from 0.29 deg in V10 slow to 0.78 deg in C10 fast; $P \leq 0.035$). In the fast condition, it was larger in V20 than in V10 ($P<0.001$). Additionally, the angle was larger in C10 than in V10 ($P \leq 0.002$). In the curb conditions, $\gamma_{wb,10}$ was larger when walking faster ($P \leq 0.042$). $\gamma_{wb,90}$ showed significant main effects for ground condition. It was significantly larger in all curb conditions compared with V0 (mean difference from 0.20 deg in V10 to 0.88 deg in C10; $P \leq 0.001$). Additionally, $\gamma_{wb,90}$ was significantly larger in V20 and C10 than in V10 ($P<0.001$). The differences between the conditions after the TD of the leading leg are illustrated in Fig. 6B. An anterior shift of 0.5 deg (V0) to 1.5 deg (C10) from 0% to 100% of the extended stride was observed.

DISCUSSION

In this study, the force direction patterns while stepping down off a visible or camouflaged curb at slow and fast walking speeds were analyzed. Although in all conditions there was the tendency to generate an IP, related variables (COM-referenced COP and GRFs) changed considerably. We did not observe a significant speed effect on the results.

Forces intersect above the COM

As was hypothesized, in all conditions the GRFs intersected above the COM. Thus, we assume that a similar stabilization strategy is used in the camouflaged curb negotiation as in the visible conditions. For the visible trials, the high R^2 (mean >97.5%) indicates that the deviation of the GRF from the calculated IP is small. The results are comparable to those of Gruben and Boehm

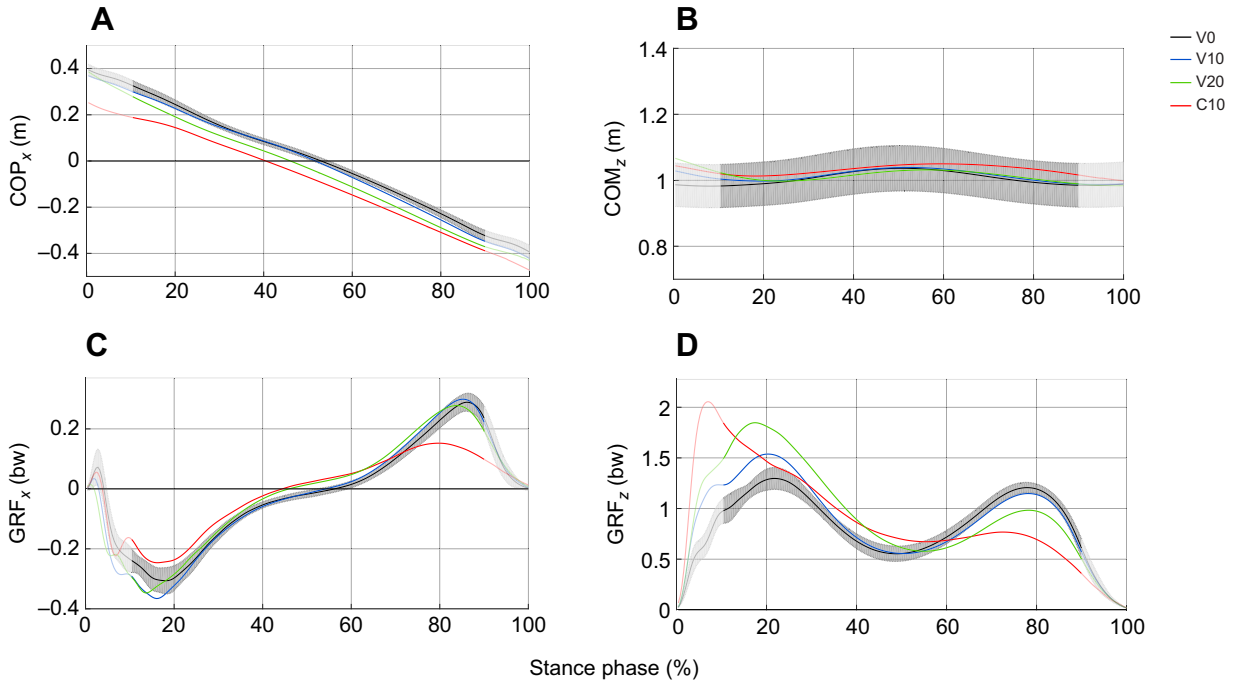

Fig. 5. Variables included in the calculation of the IP (IP-related variables). (A) Horizontal, COM-related COP position. (B) Vertical, COP-related COM position. (C) Horizontal GRFs. (D) Vertical GRFs. Mean (±s.d. for visible level walking, V0) data between the subjects (*N*=10) for fast walking (V0, V10, V20 and C10). The darker curve is 10–90% of stance phase of the leading leg, which is included in the calculations.

Journal of Experimental Biology (2019) 222, jeb204305. doi:10.1242/jeb.204305

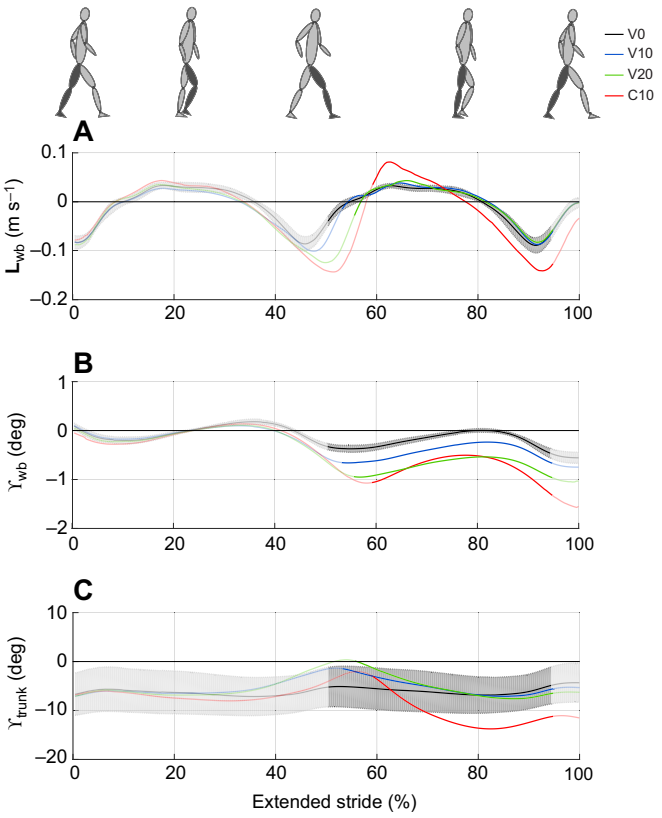

Fig. 6. Whole-body angle γ_{wb} and angular momentum L_{wb} for the extended stride. Extended stride was taken from touchdown (TD) of the trailing leg to take-off (TO) of the leading leg. Mean (±s.d. for visible level walking, V0) data between the subjects (N=10) for fast conditions (V0, V10, V20 and C10). The darker curve is 10–90% of stance phase of the leading leg. (A) L_{wb} in the sagittal plane. (B) γ_{wb} in the sagittal plane, defined as zero at mid-stance of the trailing leg. (C) Trunk angle (γ_{trunk}) in the sagittal plane. Negative values indicate a clockwise rotation.

(2012a), which also achieved high R^2 values (>98.5%) for level walking in a COM-centered reference frame. In the camouflaged conditions, the R^2 was lower than in the visible conditions. Even though the R^2 value of one subject was noticeably low in fast C10 (76.1%), the mean value was still high (>89.8%). The difference between model forces and measured forces (angle θ; Fig. 4) was higher for C10 than for the visible conditions, which produced smaller R^2 values. The graph of θ suggests higher deviations of the forces for C10 in the first two-thirds of the stance phase, with missing noticeable peaks in the beginning. A reflex-based reactive approach after the TD would probably cause short and high fluctuations early in the stance phase. It may be that in the camouflaged condition, suitable adaptations of motor behavior were made before the TD. The additional fall time to react to a camouflaged curb was short [approximately 143±23 ms for slow walking, 107±197 ms for fast walking, and 110 ms in a previous study (van Dieën et al., 2007)]. A delayed TD showed time-dependent motor adaptations in prior studies, like changes in muscle activation (walking: van der Linden et al., 2007; or running: Müller et al., 2010, 2015) or leg retraction, creating a more vertical leg position with different joint moment requirements (van Dieën et al., 2007). Both these and possibly other mechanisms could facilitate the relatively smooth transition of GRF angles to the early stance phase. To summarize, the R^2 values suggest that the GRFs pass near an IP, in both visible and camouflaged conditions.

Because the mean IP_x value was maximally up to 4 cm posterior to the COM (Table 1), the IP was located nearly on a vertical line above the COM in all conditions. Basically this agrees with the results of previous studies (Gruben and Boehm, 2012a; Maus et al., 2010; Müller et al., 2017). However, the IP_z position varies in the literature. Gruben and Boehm (2012a) observed an IP height of approximately 44±13 cm above the COM at a walking speed of 0.5 m s^{-1} (IP_z was estimated using the percentage vertical COM position of the mean body height of all subjects calculated in that study). Maus et al. (2010) calculated the IP 5–70 cm above the COM at walking speeds between 0.8 and 1.7 m s^{-1}. The IP determined by Müller et al. (2017) was located 21±7 cm above the COM at a walking speed of 1.5±0.1 m s^{-1}. Therefore, we expected a lower IP height above the COM at a higher walking speed.

In this study, the IP_z position of 18±6 cm (slow walking speed) and 15±5 cm (fast walking speed) above the COM for visible level walking matches the data of Maus et al. (2010) (lower third) and Müller et al. (2017) and is considerably below the values calculated by Gruben and Boehm (2012a). The speed effect assumed from the above-mentioned data was not observed in the speed range of this study. However, it is possible that slower or faster walking could affect IP height. Furthermore, the chosen reference frame could also have an effect on the IP position. Gruben and Boehm (2012a) evaluated a lower IP position for a hip- or body-related reference frame. Thus, comparison between the different studies should consider which reference frame was used. While the chosen reference frame of Gruben and Boehm (2012a) and Müller et al. (2017) was also COM centered and aligned to the vertical, Maus et al. (2010) used a COM-centered reference frame that was aligned to the trunk.

Presumably, there are other factors that affect the IP height. However, the trunk orientation investigated by Müller et al. (2017) does not seem to have a major effect on IP height; the mean height increases only slightly with increasing trunk inclination. Other studies (Gruben and Boehm, 2012a; Maus et al., 2010) have suggested that raising the IP increases stability but also the energy cost. Hence, a higher IP_z position in C10 compared with the visible conditions could be expected in this study to negotiate the larger perturbation. However, this was not confirmed. In addition to speed, we also examined the effect of curb height on the IP_z position. Here, we found a significantly lower IP_z position in the visible curb conditions compared with level walking. Therefore, curb height seems to be the only previously investigated factor that affects IP height.

Regulation of the IP and the whole-body angle

When calculating the IP, solely the COM-referenced COP and the GRFs in the sagittal plane were considered and thus control its position. For the GRFs, only the ratio of the horizontal and vertical components had an effect.

In the visible conditions, there were changes in the IP-related variables that could be associated with the IP height. The ratio of the GRF components seems to have the greatest effect on the IP_z position compared with the other IP-related variables. When describing it by the ratio of vertical impulse to horizontal impulse (Table 1), a decrease from V0 to the curb conditions can be observed in all cases, except the fast V20. This decrease presumably causes the lower IP height found in the curb conditions (Table 1). We noticed that most subjects negotiated the level track and the 10 cm curb (visible and camouflaged) with heel landing and the 20 cm curb with toe landing. [For visible level walking, 0% (V10: 14%, C10: 9%) of all trials were accomplish with toe landing. In the 20 cm curb condition, we observed toe landing in 64% of the trials. Toe landing was defined as proposed by Knorz et al. (2017).] This could

affect the kinetics and kinematics at landing (van Dieën et al., 2007, 2008). Gruben and Boehm (2012b, 2014) observed that, when both standing and walking, the GRFs point more anterior with the COP near the heel and more posterior with the COP near the toe. However, from a mechanical point of view a shift of the GRF independent of the COP would be required to affect the IP position. Besides mechanics, other components also produce the GRF direction during walking. For example, neural control is an important factor that coordinates the direction of the GRF by torques (Gruben and Boehm, 2014). Thus, in prior work and this study, an emergent behavior of mechanical and neural control can be suggested, which ensures that the IP_x position does not change from V10 to V20 (Gruben and Boehm, 2014).

While IP height changes were not significant in C10, the camouflaged curb condition showed the most pronounced differences in IP-related variables. The greatest of these was the horizontal shift in the COM-referenced COP in the posterior direction, which means that the COP was nearer to the COM at TD and further away at the end of the stance phase compared with the visible conditions. This asymmetrical step behavior could again be associated with a delayed TD in the perturbed step and a continuous leg retraction in this longer fall time, producing a more vertical leg position at TD (van Dieën et al., 2007). When the IP is generated in level walking, forces directed in front of the COM produce a moment angularly accelerating the body in the posterior direction and forces behind the COM produce a moment angularly accelerating the body in the anterior direction, until force angle and COM are aligned. Note that γ_{wb} is in a more anterior rotation at TD in C10 compared with V0 and V10 (Fig. 6B). The COP posterior shift would allow less time to generate a posterior moment and more time to generate an anterior moment and therefore complicate the handling of the perturbed body state. However, in our discussion so far, changes in the force amplitude have not been considered. In C10, there were higher vertical forces in the beginning of the stance phase and lower vertical forces in the second half of the stance phase (Fig. 5D). This asymmetrical force behavior partially counters the effect of a higher anterior rotated γ_{wb} prior to the TD, as in this case higher forces at the beginning can produce higher moments for posterior rotation in the shortened time frame. With all these changes, γ_{wb} did not return to level walking range values, remaining more anterior even in the visible curb conditions. This could possibly be compensated in later steps.

Future considerations

While the VPP model assumes exactly one single point as the IP, the experimentally measured forces intersect with spread around one point, so that an intersection area of force vectors occur. However, no one has clearly defined up to what spread the intersection area can still be denoted as a point as introduced by the model. That would have to be examined in a simulation of the model with an intersection area instead of an intersection point. We suggest the R^2 as defined by Herr and Popovic (2008) rather than the squared distance r (Maus et al., 2010; Müller et al., 2017) to determine the accuracy of intersection, because it normalizes the spread with regard to variability of the measured variables and is comparable between the studies. Here, the angle approach seems to be more suitable than the force approach proposed by Herr and Popovic (2008), because it disregards the magnitude of the forces. Nevertheless, there is no clear limit up to which value of R^2 the intersection area can be denoted as a point. These limits should be methodically researched and specified.

Another methodological problem is the definition of the included single stance time. The constant cutting off of 10% as performed in previous studies (Andrada et al., 2014; Müller et al., 2017) does not represent the exact single support phase. This can also be observed in the graph of the angle θ between model forces and experimentally measured GRFs (Fig. 4), which indicates that the deviations mainly occur at the beginning and the end of the considered contact time. This possibly represents a superposition of the GRFs at double stance phase. However, considering the pure single support phase, the different contact and t_{double} (Table 2) in the visible versus camouflaged conditions would affect the position and precision of the IP and make conditions less comparable. Furthermore, it might also be worth analyzing the IP for the double stance phase.

A limitation of this study is that the subjects could have chosen a new strategy that differs from level-ground walking because they were aware of the possible perturbation. Future studies might consider investigating larger curb heights or other perturbations to the angular momentum. Noteworthy is a study in which subjects tripped over an unexpected obstacle at mid-stance phase (Pijnappels et al., 2004). The high moment in the anterior direction produced by tripping was countered by some subjects with a posterior moment in the second half of the stance phase. As force vectors would be below the COM here, this force regulation suggests the possibility of other control strategies. One possibility would be that the IP is just an emerging variable, where another control strategy would produce the IP as a side effect. This assumption is supported by experimental and modeling approaches (Gruben and Boehm, 2014; Maus et al., 2010; Müller et al., 2017; Rummel and Seyfarth, 2010; Sharbafi and Seyfarth, 2015). Gruben and Boehm (2014) showed the IP above the COM to be an emerging variable produced by the interaction of (a) ankle torques that generate the typical heel-to-toe roll-over and (b) a neural coordination of the remaining joint torques. The resulting behavior, it was argued, has favorable energetic and stability properties. There could be a switch in the neural control approach for highly perturbed situations. A more precise determination of different control strategies could be the subject of future studies.

These experiments could also be adapted for the elderly or patients with a neurological disorder, because they have a higher risk of falling (Berg et al., 1997; Menz et al., 2003). Additionally, it may be investigated whether the proximity of the GRF lines of action to the calculated IP could be used as a stabilizing parameter for walking.

Acknowledgements

We would like to thank Isabel Kolkka, Christian Rimpau and Will Murray for proof reading the manuscript.

Competing interests

The authors declare no competing or financial interests.

Author contributions

Conceptualization: R.M.; Methodology: J.V., E.G., R.M.; Software: J.V., E.G.; Validation: J.V., E.G., R.M.; Formal analysis: J.V., E.G.; Investigation: J.V., E.G., R.M.; Data curation: J.V., E.G.; Writing - original draft: J.V., E.G.; Writing - review & editing: J.V., E.G., R.M.; Visualization: J.V., E.G.; Supervision: R.M.; Project administration: R.M.; Funding acquisition: R.M.

Funding

This project was supported by the Deutsche Forschungsgemeinschaft (MU 2970/4-1 to R.M.).

Data availability

Kinetic and kinematic data are available from the figshare repository: https://doi.org/10.6084/m9.figshare.7558586.v1

Supplementary information

Supplementary information available online at
http://jeb.biologists.org/lookup/doi/10.1242/jeb.204305.supplemental

References

Alexander, R. M. N. (1995). Simple models of human movement. *Appl. Mech. Rev.* **48**, 461-470. doi:10.1115/1.3005107

Aminiaghdam, S., Rode, C., Müller, R. and Blickhan, R. (2017). Increasing trunk flexion transforms human leg function into that of birds despite different leg morphology. *J. Exp. Biol.* **220**, 478-486. doi:10.1242/jeb.148312

AminiAghdam, S., Griessbach, E., Vielemeyer, J. and Müller, R. (2019). Dynamic postural control during (in)visible curb descent at fast versus comfortable walking velocity. *Gait Posture* **71**, 38-43. doi:10.1016/j.gaitpost.2019.04.014

Andrada, E., Rode, C., Sutedja, Y., Nyakatura, J. A. and Blickhan, R. (2014). Trunk orientation causes asymmetries in leg function in small bird terrestrial locomotion. *Proc. R. Soc. B* **281**, 20141405. doi:10.1098/rspb.2014.1405

Berg, W. P., Alessio, H. M., Mills, E. M. and Tong, C. (1997). Circumstances and consequences of falls in independent community-dwelling older adults. *Age Ageing* **26**, 261-268. doi:10.1093/ageing/26.4.261

Buckley, J. G., MacLellan, M. J., Tucker, M. W., Scally, A. J. and Bennett, S. J. (2008). Visual guidance of landing behaviour when stepping down to a new level. *Exp. Brain Res.* **184**, 223-232. doi:10.1007/s00221-007-1096-8

Capaday, C. (2002). The special nature of human walking and its neural control. *Trends Neurosci.* **25**, 370-376. doi:10.1016/S0166-2236(02)02173-2

Gruben, K. G. and Boehm, W. L. (2012a). Force direction pattern stabilizes sagittal plane mechanics of human walking. *Hum. Mov. Sci.* **31**, 649-659. doi:10.1016/j.humov.2011.07.006

Gruben, K. G. and Boehm, W. L. (2012b). Mechanical interaction of center of pressure and force direction in the upright human. *J. Biomech.* **45**, 1661-1665. doi:10.1016/j.jbiomech.2012.03.018

Gruben, K. G. and Boehm, W. L. (2014). Ankle torque control that shifts the center of pressure from heel to toe contributes non-zero sagittal plane angular momentum during human walking. *J. Biomech.* **47**, 1389-1394. doi:10.1016/j.jbiomech.2014.01.034

Herr, H. and Popovic, M. (2008). Angular momentum in human walking. *J. Exp. Biol.* **211**, 467-481. doi:10.1242/jeb.008573

Hof, A. L. (1996). Scaling gait data to body size. *Gait Posture* **4**, 222-223. doi:10.1016/0966-6362(95)01057-2

Knorz, S., Kluge, F., Gelse, K., Schulz-Drost, S., Hotfiel, T., Lochmann, M., Eskofier, B. and Krinner, S. (2017). Three-dimensional biomechanical analysis of rearfoot and forefoot running. *Orthopaedic J. Sports Med.* **5**, 2325967117719065. doi:10.1177/2325967117719065

Lee, J., Vu, M. N. and Oh, Y. (2017). A control method for bipedal trunk spring loaded inverted pendulum model. in 13th international conference on autonomic and autonomous systems (ICAS 2017) (ed. C. B. Westphall, M. Mendonca and R. O. Vasconcelos), pp. 24-29. Barcelona, May 21-25, 2017.

Maus, H.-M., Rummel, J. and Seyfarth, A. (2008). Stable upright walking and running using a simple pendulum based control scheme. In *Advances in Mobile Robotics* (ed. L. Marques, A. T. de Almeida, M. O. Tokhi and G. S. Virk), pp. 623-629. World Scientific.

Maus, H.-M., Lipfert, S. W., Gross, M., Rummel, J. and Seyfarth, A. (2010). Upright human gait did not provide a major mechanical challenge for our ancestors. *Nat. Commun.* **1**, 70. doi:10.1038/ncomms1073

Menz, H. B., Lord, S. R. and Fitzpatrick, R. C. (2003). Acceleration patterns of the head and pelvis when walking are associated with risk of falling in community-dwelling older people. *J. Gerontol. Ser. A Biol. Sci. Med. Sci.* **58**, M446-M452. doi:10.1093/gerona/58.5.M446

Müller, R., Grimmer, S. and Blickhan, R. (2010). Running on uneven ground: leg adjustments by muscle pre-activation control. *Hum. Mov. Sci.* **29**, 299-310. doi:10.1016/j.humov.2010.01.003

Müller, R., Tschiesche, K. and Blickhan, R. (2014). Kinetic and kinematic adjustments during perturbed walking across visible and camouflaged drops in ground level. *J. Biomech.* **47**, 2286-2291. doi:10.1016/j.jbiomech.2014.04.041

Müller, R., Häufle, D. F. B. and Blickhan, R. (2015). Preparing the leg for ground contact in running: the contribution of feed-forward and visual feedback. *J. Exp. Biol.* **218**, 451-457. doi:10.1242/jeb.113688

Müller, R., Rode, C., Aminiaghdam, S., Vielemeyer, J. and Blickhan, R. (2017). Force direction patterns promote whole body stability even in hip-flexed walking, but not upper body stability in human upright walking. *Proc. R. Soc. A* **473**, 20170404. doi:10.1098/rspa.2017.0404

Nielsen, J. B. (2003). How we walk: central control of muscle activity during human walking. *Neuroscientist* **9**, 195-204. doi:10.1177/1073858403009003012

Peng, J., Fey, N. P., Kuiken, T. A. and Hargrove, L. J. (2016). Anticipatory kinematics and muscle activity preceding transitions from level-ground walking to stair ascent and descent. *J. Biomech.* **49**, 528-536. doi:10.1016/j.jbiomech.2015.12.041

Pijnappels, M., Bobbert, M. F. and van Dieën, J. H. (2004). Contribution of the support limb in control of angular momentum after tripping. *J. Biomech.* **37**, 1811-1818. doi:10.1016/j.jbiomech.2004.02.038

Pijnappels, M., Bobbert, M. F. and van Dieën, J. H. (2005). Push-off reactions in recovery after tripping discriminate young subjects, older non-fallers and older fallers. *Gait Posture* **21**, 388-394. doi:10.1016/j.gaitpost.2004.04.009

Plagenhoef, S., Evans, F. G. and Abdelnour, T. (1983). Anatomical data for analyzing human motion. *Res. Q Exerc. Sport* **54**, 169-178. doi:10.1080/02701367.1983.10605290

Reeves, N. D., Spanjaard, M., Mohagheghi, A. A., Baltzopoulos, V. and Maganaris, C. N. (2008). The demands of stair descent relative to maximum capacities in elderly and young adults. *J. Electromyogr. Kinesiol.* **18**, 218-227. doi:10.1016/j.jelekin.2007.06.003

Roos, P. E. and Dingwell, J. B. (2013). Using dynamic walking models to identify factors that contribute to increased risk of falling in older adults. *Hum. Mov. Sci.* **32**, 984-996. doi:10.1016/j.humov.2013.07.001

Rummel, J. and Seyfarth, A. (2010). Passive stabilization of the trunk in walking. In Proceedings of SIMPAR 2010 Workshops: International Conference on Simulation, Modeling, and Programming for Autonomous Robots, Darmstadt, Germany, 15–16 November 2010, Darmstadt, Germany: Technische Universität Darmstadt.

Sharbafi, M. A. and Seyfarth, A. (2015). Fmch: a new model for human-like postural control in walking. In IEEE/RSJ International Conference on Intelligent Robots and Systems (IROS), pp. 5742-5747. IEEE.

Silverman, A. K., Neptune, R. R., Sinitski, E. H. and Wilken, J. M. (2014). Whole-body angular momentum during stair ascent and descent. *Gait Posture* **39**, 1109-1114. doi:10.1016/j.gaitpost.2014.01.025

van der Linden, M. H., Marigold, D. S., Gabreëls, F. J. M. and Duysens, J. (2007). Muscle reflexes and synergies triggered by an unexpected support surface height during walking. *J. Neurophysiol.* **97**, 3639-3650. doi:10.1152/jn.01272.2006

van Dieën, J. H., Spanjaard, M., Konemann, R., Bron, L. and Pijnappels, M. (2007). Balance control in stepping down expected and unexpected level changes. *J. Biomech.* **40**, 3641-3649. doi:10.1016/j.jbiomech.2007.06.009

van Dieën, J. H., Spanjaard, M., Könemann, R., Bron, L. and Pijnappels, M. (2008). Mechanics of toe and heel landing in stepping down in ongoing gait. *J. Biomech.* **41**, 2417-2421. doi:10.1016/j.jbiomech.2008.05.022

Winter, D. A. (1995). Human balance and posture control during standing and walking. *Gait Posture* **3**, 193-214. doi:10.1016/0966-6362(96)82849-9

Winter, D. A. (2009). *Biomechanics and Motor Control of Human Movement.* John Wiley & Sons.